ELSEVIER

Composites Science and Technology 60 (2000) 2681–2691

COMPOSITES SCIENCE AND TECHNOLOGY

www.elsevier.com/locate/compscitech

The effect of stitching on the low-velocity impact response of delaminated composite beams

Bhavani V. Sankar *, Huasheng Zhu

Department of Aerospace Engineering, Mechanics & Engineering Science, PO Box 116250, University of Florida, Gainesville, FL 32611, USA

Received 7 December 1999; received in revised form 4 May 2000; accepted 6 June 2000

Abstract

A numerical simulation is performed to predict the effects of stitching on the low-velocity impact response of stitched delaminated beams. The load/displacement relations during the impact are assumed to be the same as in the corresponding static problem. Hence a solution to the problem of a stitched delaminated beam under a static contact force is developed. The effects of stitches are modeled as a constant shear traction in the stitch bridging zone to account for the shear resistance offered by the unbroken stitches. From the static simulation the load/displacement and displacement/crack-extension relations are obtained. From the area under the load/deflection diagram the apparent fracture toughness due to the stitching is also estimated. The impact simulations provide information on the load at which the crack propagation initiates, the maximum contact force, and the extent of crack propagation at the end of the impact event. The results indicate that stitching does not increase the load at which delamination begins to propagate, but greatly reduces the extent of delamination growth at the end of the impact event.

Keywords: Composite bean; Crack propagation; Delamination; Low velocity impact; Stitching of laminates

1. Introduction

Currently various types of translaminar reinforcements are being studied in order to improve the interlaminar strength and fracture toughness of both composite laminates [1], and sandwich constructions [2]. A comprehensive study by Sharma and Sankar [3] demonstrated that stitching is very effective in improving the compression-after-impact (CAI) strength and Mode I fracture toughness of carbon/epoxy laminates, and moderately effective in improving the Mode II fracture toughness. Sharma and Sankar found that stitching did not significantly increase the impact-energy threshold for initiation of damage. However the extent of delamination at the end of impact was reduced as a result of the stitching. This effect was again not significant in thin laminates, whereas Poe et al. [4] found that stitching improves the impact resistance of thicker laminates. Similar findings have been reported by Dexter and Funk [5] and Peistring and Madan [6].

There have been several analytical studies on the prediction of the effects of stitching on the fracture toughness of composite laminates [7–11]. In the present paper we have developed an analytical model to predict the effectiveness of stitching on improving the impact properties of composite laminates. An impact simulation is performed to determine the maximum contact force and extent of delamination propagation in a stitched laminate due to low-velocity impact. Various stitch parameters such as stitch density are considered and the results are compared to unstitched laminates also. As part of the study, the corresponding static problem was also considered. The beam was subjected to a static force and quasi-static delamination propagation was studied. From these results one can obtain results for the apparent Mode II fracture toughness of stitched specimens. The results indicate that stitching is effective in reducing the delamination area due to low-velocity impact.

Conventionally, stitches have been modeled as linear elements, either as uniaxial bar or beam. The stiffness of the stitch elements can be either linear up to failue or non-linear to account for inelastic effects. Such models are useful when the stitches are under Mode I fracture. A major difference between the impact loading and the

* Corresponding author. Tel.: +1-352-392-6749; fax: +1-352-392-7303.

E-mail address: sankar@ufl.edu or sankar@aemes.aero.ufl.edu (B.V. Sankar).

0266-3538/00/$ - see front matter
PII: S0266-3538(00)00132-9

inplane compressive loading (CAI Test) is that the delamination is under pure Mode II (shearing mode) conditions during impact, whereas it is predominantly under Mode I during sublaminate buckling in CAI tests. Previous experimental studies by Sharma and Sankar [3] have found that under pure Mode II, the stitches try to plough through the matrix material, and the resistance offered by the matrix is responsible for increase in apparent fracture toughness. Thus the stitch model has to be modified in impact problems to account for the "ploughing" phenomenon.

2. Analytical model

2.1. Basic assumptions

Several assumptions are made to simplify the impact simulation. Some of these assumptions are typical of low-velocity impact problems [12]. The assumptions regarding stitch modeling are based on the experimental observations of Sharma and Sankar [3]. The assumptions are as follows:

1. The velocity of impact is low compared to the velocities of wave propagation in the composite beam;
2. The projectile is assumed to be rigid compared to the target. Therefore the impactor can be treated as a rigid body and thus its equation of motion will be greatly simplified;
3. The target, laminated beam in the present case, is highly flexible. That is, the deflection of the beam is expected to be much higher than the local indentation, and hence the Hertzian indentation effects can be neglected;
4. The impactor mass is much greater than that of the beam, and hence the impact duration will be very long compared to the fundamental period of vibration of the beam. Therefore the target can be represented by a simple spring/mass system. The stiffness of the spring can be approximated by the static beam stiffness k at the impact location;
5. A central delamination is assumed to be pre-existing in the laminated beam. The delamination is symmetrically located in the simply supported beam (see Fig. 1). The distance of the delamination from the laminate mid-plane is considered as a variable in this study.

Because of Assumption 4 above, we need to compute only the static stiffness of the delaminated stitched beam as a result of central transverse force.

We will assume that the delamination will propagate along the same plane when the energy-release rate G exceeds G_{IIc}, the Mode II fracture toughness of the parent laminate. As the delamination propagates the stitches in the wake of delamination will undergo strains leaving a crack-bridging zone behind the crack-tip. The crack-bridging tractions are assumed to be a constant. The crack-bridging forces are essentially the resistance offered by the matrix as the stitches tend to plough through the matrix. The ploughing resistance of the stitches can be represented as a distributed shear traction (force/unit length) at the interface of the two sublaminates that are stitched together. The traction p_0 is estimated as

$$p_0 = \frac{B}{S}\frac{Dh\sigma_y}{n} \tag{1}$$

where B is the beam width, D is diameter of stitch yarn, h is the lesser of the two sublaminate thicknesses, σ_y, is yield stress of the surrounding matrix, S is the stitch spacing in the width direction and n is the number of stitches per inch. In terms of stitch density the distributed traction can be written as:

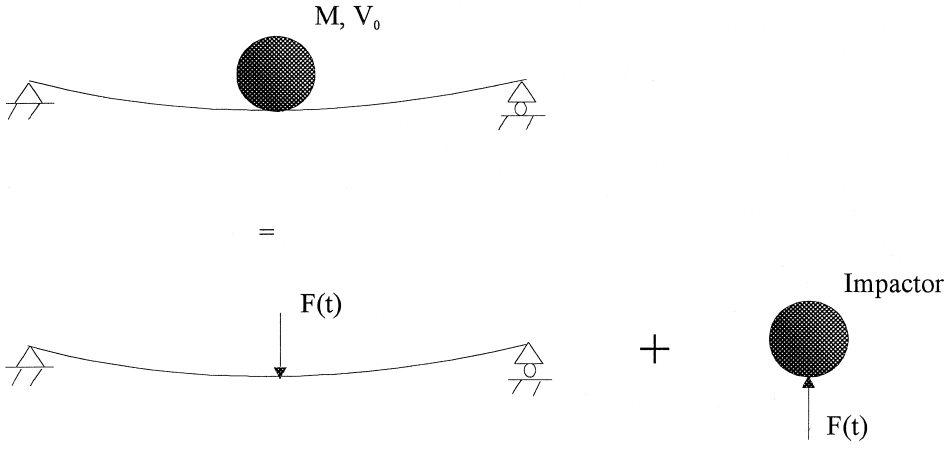

Fig. 1. A beam under impact.

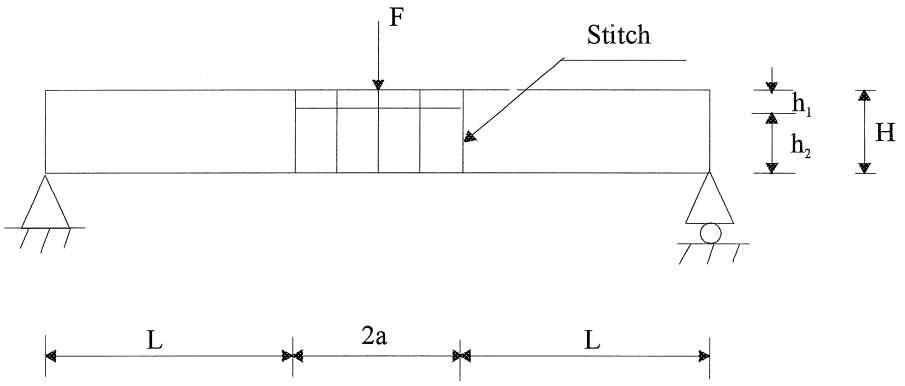

Fig. 2. A delaminated beam with stitches subject to impact load F.

$$p_0 = NBDh\sigma \tag{2}$$

where $N = 1/(n \times S)$ is the number of stitches per unit area of the laminate. As the delamination propagates new stitches come into action in the freshly created delamination areas, and they offer additional shear resistance. This assumption is consistent with the experimental observations of Sharma and Sankar [3]. It should be mentioned that many other models can be developed to represent the shear tractions, however the focus of this study is to understand their effects on the impact response.

2.2. Impact equations

The equation of motion of the impactor along with the initial conditions can be written as:

$$M_0 \frac{d^2q}{dt^2} = -F(q) \tag{3}$$

$$q(0) = 0 \tag{4}$$

$$\frac{dq}{dt}|_{t=0} = V_0 \tag{5}$$

where M_0 is the impactor mass, q is the impactor displacement which is same as the transverse deflection of the target beam at the point of impact, V_0 is the initial velocity of the impactor or the impact velocity, and $F(q)$ is the contact force. The contact force F is a function of the beam deflection. The contact force, F, will be a linear function of q if there were no stitches or delamination propagation. However, in the present case it will be a non-linear function. Once $F(q)$ is determined, then the equations of motion [Eqs. (3)–(5)] can be numerically integrated to obtain $q(t)$. From $q(t)$ one can compute the impact force history, $F(t)$, using the F/q relationship. In the following section, we discuss the procedure for determining the F/q relationship in a stitched delaminated beam.

2.3. Static force/deflection relation

The problem to be solved in this section is depicted in Fig. 2. The problem is to find the relation between transverse force F and deflection q at the center of the beam in the delaminated stitched beam. Further, the energy-release rate G at the crack-tip needs to be computed also. In the numerical simulation, the crack will be propagated by a small distance (symmetrically on both sides), if the G exceeds G_{IIc} of the parent laminated material system.

First, we will provide an overview of the procedures to be followed. Since the structure is symmetric we can analyze the right half of the beam as shown in Fig. 3. The half-crack length is denoted by a and L is the length of the intact beam as shown in Fig. 3.The right half beam can be divided into three elements: elements 1, 2 and 3 denoted as $<1>$, $<2>$ and $<3>$ in Fig. 3. Free body diagrams of the three elements are shown in Fig. 4. The x-axis is along the length of the beam and the z-axis is the thickness direction. At each node (end) of the element there are three displacements, u, w and ψ and three corresponding forces, F_x, F_z and C. The u and w are the displacements in the x and z directions and ψ is the rotation of the cross-section. F_{xi} and F_{zi} are external forces in the axial direction and transverse direction, respectively, and C_i is the nodal couple corresponding to the rotation ψ. Odd indices $i(i = 1, 3, 5)$ denote the

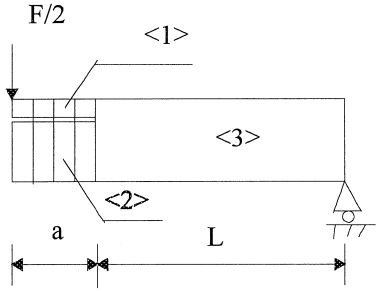

Fig. 3. Right half side of specimen in Fig. 2 and the three sub-laminates.

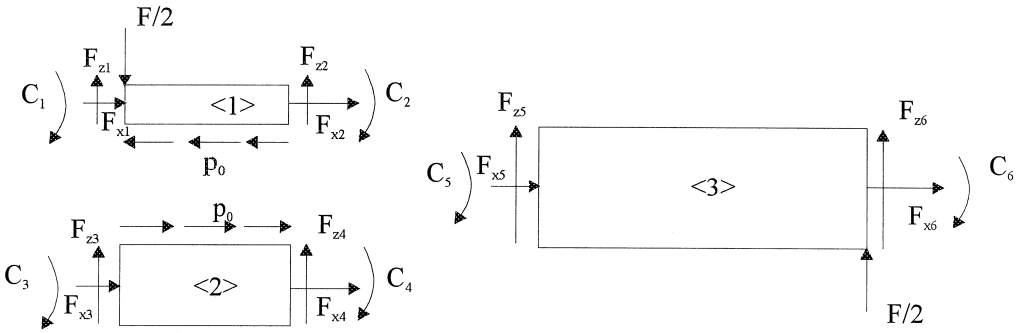

Fig. 4. Free body diagrams of sublaminates <1>, <2> and <3>.

left end node of each element and even indices ($i = 2, 4, 6$) correspond to the right end nodes.

We use the shear deformable beam theory in modeling the beams. The differential equations of equilibrium of a general element are given in Appendix A. These equations can be easily solved as described in Appendix A to obtain a relation between the six forces acting at the two nodes of the element and the six corresponding displacements. In order to relate the forces in the three different elements we use force and moment equilibrium equations, and compatibility equations at the junctions (common node) where the three elements meet. Further, the boundary conditions at the ends of the beam can also be implemented. This procedure is similar to assembling elements in the finite element method except the stiffness matrix of each element is obtained exactly by solving the differential equations of equilibrium. The forces and displacements in each element are shown in Fig. 4. It should be noted that F is the contact force acting on the beam, and because of symmetry $F/2$ is assumed to act at Node 1 of Element 1. The compatibility relation for the axial displacements at the common node is depicted in Fig. 5.

The force and moment equilibrium equations, the compatibility equation and boundary conditions are as follows. Force and moment equilibrium equations are:

$$F_{x2} + F_{x4} + F_{x5} = 0 \tag{6}$$

$$F_{z1} + F_{z3} = -\frac{F}{2} \tag{7}$$

$$F_{z2} + F_{z4} + F_{z5} = 0 \tag{8}$$

$$C_2 + C_4 + C_5 + F_{x2}\frac{h_2}{2} - F_{x4}\frac{h_1}{2} = 0 \tag{9}$$

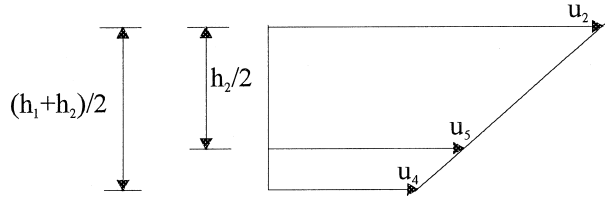

Fig. 5. Compatibility of displacements in axial direction at the junction between the three sublaminates.

Compatibility equations at the common nodes are:

$$u_2 = u_5 + \frac{h_2}{2}\psi_5 \tag{10}$$

$$u_4 = u_5 - \frac{h_1}{2}\psi_5 \tag{11}$$

$$w_2 = w_4 = w_5 \tag{12}$$

$$\psi_2 = \psi_4 = \psi_5 \tag{13}$$

Boundary conditions:

$$u_1 = u_3 = 0 \tag{14}$$

$$\psi_1 = \psi_3 = 0 \tag{15}$$

$$w_1 = w_6 \tag{16}$$

$$w_6 = F_{x6} = C_6 = 0 \tag{17}$$

Expressions of F_{xi}, F_{zi} and C_i are derived in Appendix A.

After implementing the aforementioned element equilibrium conditions and displacement compatibility conditions at the nodes, a compact set of five equations are obtained for the five displacements w_1, u_5, w_5, ψ_5 and ψ_6 as shown in Eq. (18).

$$\begin{bmatrix} k_{11} & k_{12} & k_{13} & k_{14} & k_{15} \\ k_{21} & k_{22} & k_{23} & k_{24} & k_{25} \\ k_{31} & k_{32} & k_{33} & k_{34} & k_{35} \\ k_{41} & k_{42} & k_{43} & k_{44} & k_{45} \\ k_{51} & k_{52} & k_{53} & k_{54} & k_{55} \end{bmatrix} \begin{Bmatrix} w_1 \\ u_5 \\ w_5 \\ \psi_5 \\ \psi_6 \end{Bmatrix} = \begin{Bmatrix} f_1 \\ f_2 \\ f_3 \\ f_4 \\ f_5 \end{Bmatrix} \tag{18}$$

The stiffness coefficients $k_{ij}(i = 1, 5, j = 1, 5)$ and the generalized forces $f_1 \ldots f_5$ on the right hand side of Eq. (18) are given in Appendix B.

In Eq. (18) the forces $f_2 \ldots f_5$ are known. The force f_1, related to the contact force F, by $f_1 = F/2$, is the unknown. On the other hand, the deflection w_1 (same as the variable q used in impact equations) can be treated as known, and the other five displacements are

unknowns. Thus we have five equations for five unknowns. The equations can be solved for a given w_1 to determine f_1 or the contact force/displacement F/q relations can be developed. The flowchart in Fig. 6 describes the procedure used in developing the F/q relations.

2.4. Energy-release rate calculation

At each displacement increment the energy-release rate G is computed using the procedure explained in the next paragraph. If the value of G exceeds the Mode II fracture toughness G_{IIc}, the length of the delamination is increased by a small amount. The numerical value of the extension is arrived by an interative method until G equals G_{IIc} for that deflection increment.

In order to compute the G, we used the strain-energy density method derived by Sankar [13] and then later used by Sankar and Sonik [14] and Sankar and Park [15] for computing the point-wise energy-release rate in delaminated plates. This method is very much suitable for the present model as the force and moment resultants ahead and behind the crack-tip can be obtained in a closed-form from the solution of the differential equations of equilibrium, and the energy-density values thus calculated are very accurate. Consider the three elements surrounding the crack-tip as shown in Fig. 3. There are two (Elements 1 and 2) behind the crack-tip and one ahead of the crack-tip (Element 3). The G is derived as:

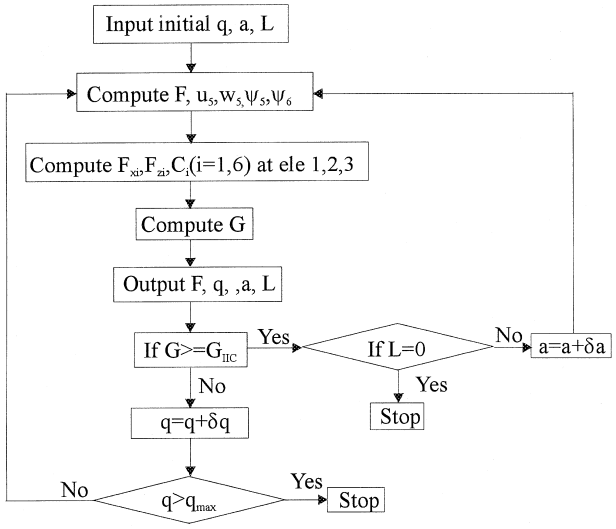

a: Crack length

L: Uncracked length

F: Contact force

q: Deflection at center point

G: Energy release rate

Fig. 6. Flow chart for computing the F/q relations.

$$G = \frac{1}{B}\left(U_{\mathrm{L}}^{(1)} + U_{\mathrm{L}}^{(2)} - U_{\mathrm{L}}^{(3)}\right) \tag{19}$$

where U_{L} represents the strain-energy density per unit length of the beam, and the superscripts (1) and (2) denote the cross-sections immediately behind the crack tip and (3) denotes the cross-section immediately ahead of the crack-tip and B is the width of the beam in the y-direction. The strain-energy density in terms of force and moment resultants is given by:

$$U_{\mathrm{L}} = \frac{1}{2}\left(\frac{P^2}{EA} + \frac{M^2}{EI} + \frac{V^2}{GA}\right) \tag{20}$$

where P, M and V are the axial force, bending moment and shear force resultants; EA, EI and GA are the equivalent axial, flexural and shear rigidities of the beam cross-section.

2.5. Impact simulations

After computing the F/q relation for a beam, the impact equations [Eqs. (3)–(5)] can be solved numerically. The F/q relations computed from the static analysis were stored in a spread sheet program (Excel^{TM}). The expression for $F(q)$ on the RHS of Eq. (3) can be approximated by a linear interpolation in each small step as:

$$F(q) = F_1 + \frac{F_2 - F_1}{(q_2 - q_1)}(q - q_1) \tag{21}$$

where q_1 and q_2 are impactor initial and final displacements and F_1 and F_2 are initial and final contact force in each step.

From Eq. (3), a relation between contact force F and velocity V can derived as follows:

$$M\frac{\mathrm{d}}{\mathrm{d}t}\left(\frac{\mathrm{d}q}{\mathrm{d}t}\right) = -F(q) \tag{22}$$

where

$$\frac{\mathrm{d}q}{\mathrm{d}t} = V \tag{23}$$

Substituting from Eq. (23) into Eq. (22) and modifying the resulting equation a new equation, relating the contact force $F(q)$ and the impact velocity V can be obtained as

$$M\frac{\mathrm{d}V}{\mathrm{d}q}\frac{\mathrm{d}q}{\mathrm{d}t} = -F(q) \tag{24}$$

Substituting from Eq. (23) into Eq. (24) and integrating both sides of the equation, the relation between V and $F(q)$ can be derived as:

$$\frac{1}{2}M\left(V_2^2 - V_1^2\right) = -\int_{q_1}^{q_2} F(q)\mathrm{d}q \tag{25}$$

Substituting from Eq. (21) into Eq. (25) the velocity can be expressed in following form:

$$V_2 = \sqrt{V_1^2 - \frac{1}{M}(q_2 - q_1)(F_1 + F_2)} \tag{26}$$

where V_1 and V_2 are the initial and final velocities in each step.

The corresponding impact time can be derived using Eq. (23) by assuming that the impact velocity in each step varies linearly:

$$V(q) = V_1 + \frac{V_2 - V_1}{q_2 - q_1}(q - q_1) \tag{27}$$

where q_1 and q_2 are impactor initial and final displacements in each step. Substituting Eq. (27) into Eq. (23) we derive the following integral equation:

$$\int_{t_1}^{t_2} \mathrm{d}t = \int_{q_1}^{q_2} \frac{\mathrm{d}q}{V(q)} = \int_{q_1}^{q_2} \frac{\mathrm{d}q}{V_1 + \dfrac{(V_2 - V_1)(q - q_1)}{(q_2 - q_1)}} \tag{28}$$

Integrating Eq. (28), an expression for time t_2 can be obtained as:

$$t_2 = t_1 + \frac{(q_2 - q_1)}{(V_2 - V_1)} \ln \frac{V_2}{V_1} \tag{29}$$

where t_1 and t_2 are initial and final time in each integration step. Eq. (29) provides the q/t relation for the impact problem. From that, using F/q relations, we can obtain the F/t relation or the impact force history. Since we know the delamination length at each displacement in the static problem, i.e. a/q relation, we can translate that into a/t relation, and thus the propagation of delamination can be followed.

3. Numerical examples, results and discussion

The specimen dimension and material properties used in the impact simulation are as follows: half-length of the beam = 101.6 mm, initial crack length $a_0 = 27.4$ mm, beam width $B = 25.4$ mm, equivalent Young's modulus $E_{eq} = 90.375$ GPa, and equivalent shear modulus $G_{xy} = 6.8$ GPa. Stitching material is 3570 denier[1] glass yarn and yield strength of the matrix is 40 MPa. The properties of the laminate and stitch yarn are obtained from Sharma and Sankar [3]. Nine different examples were studied. In these examples, the impactor mass, impact velocity, position of the delamination in the thickness direction and the Mode II fracture toughness G_{IIc} were varied. The parameters used in these examples are listed in Table 1.

In Table 1, H is the total thickness of the beam and h_1 is the distance of delamination from the top surface (impact surface). For each example three different cases — beam w/o stitching, 16 stitches per square inch (ssi) stitches, and 64 ssi stitches — were considered. Thus a total of 27 impact simulations were performed. The simulations were stopped when the contact force becomes equal to zero denoting the contact between the impactor and the beam has ceased. In two cases (Example 2, w/o stitches and 16 ssi stitches) the simulation has to be stopped when the delamination propagated all the way to the ends of the beam.

From the static analysis we obtain the load/deflection relation (F/q) and the delamination/deflection relation (a/q). Sample F/q relations for Example 1 are shown in Fig. 7. The F/q relation is linear until the crack begins

Table 1
Various parameters used in numerical examples[a]

Example	M_0 (kg)	V_0 (m/s)	T (J)	Position of delamination (h_1/H)	G_{IIc} (J/m^2)
1	5	1.5	5.625	0.5	530
2	5	*1.5*	5.625	0.5	300
3	1.25	3	5.625	0.5	530
4	2.5	1.5	2.813	0.5	530
5	2.5	1.5	2.813	0.5	300
6	5	1.5	5.625	0.25	530
7	5	1.5	5.625	0.25	300
8	2.5	1.5	2.813	0.25	530
9	2.5	1.5	2.813	0.25	300

[a] m_0, Impactor mass; V_0, impact velocity; T, impact energy.

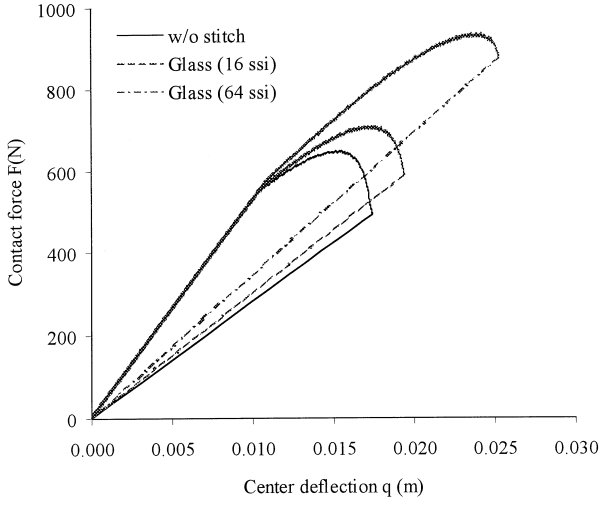

Fig. 7. Contact force F versus center deflection q for $G_{IIc} = 530$ J/m^2.

[1] Denier is a measure of yarn linear density, and it is equal to the mass in grams of 9000 m of yarn.

to propagate. It may be noted that the load at which the crack begins to propagate is almost the same for all three cases (w/o stitches, 16 ssi and 64 ssi stitches). After that the curves take different shapes depending on the stitch density. The maximum load that the beam can carry very much depends on the stitch density. The 64 ssi beam carries about 50% more load than the unstitched beam. The unloading was assumed to be linear and hence the unloading curve was a straight line joining the origin. This assumption is validated by the Mode II experiments conducted by Sharma and Sankar [3,16].

Another interesting result that can be deduced from the static load/deflection curve is the apparent fracture toughness of stitched laminates. The area enclosed by the load/deflection diagram (Fig. 7) denotes the work of fracture. Since we know the extent of delamination propagation we can compute the apparent fracture toughness G_{Iicap} from:

$$G_{\text{IIcap}} = \frac{\Delta W}{\Delta A}$$

where ΔW is the work done and ΔA is the new delamination surface created. The apparent fracture toughness for various cases is presented in Table 2 along with that for unstitched laminates. The numbers in parentheses are the percentage increase in apparent fracture toughness. It may be seen that the percentage increase in G_{IIc} is higher for laminates with lower fracture toughness.

The results for each impact analysis include the complete impact force history (F/t) and the delamination propagation history (a/t). A sample impact-force history is shown in Fig. 8. In general stitched beams carry more impact force, provided the impact energy is sufficient to cause delamination propagation. For low impact energies, the impact-force history will be identical in stitched and unstitched beams, because the stitches come into effect only when there is sufficient energy to propagate the delamination.

The results presented in Table 3 show for each case, the impact energy, G_{IIc} of the parent material system, the contact force F_i at which the delamination began to propagate, the final crack length $a_{\max}$ and the maximum contact force $F_{\max}$ during the impact event. The extent of delamination propagation is also shown in the bar charts in Figs. 9 and 10. Fig. 9 considers the examples

Table 2
Effect of stitching on the apparent $G_{\text{IIc}}(G_{\text{IICAp}})$[a]

Case	G_{IIc} (J/m^2)	G_{IIcAp} for 16 ssi[b]	G_{IIcAp} for 64 ssi[b]
1	530	595 (12%)	707 (33%)
2	300	344 (15%)	430 (43%)

[a] Numbers in parentheses indicate percentage increase in G_{IIc} due to stitching.
[b] ssi, Stitches per square inch.

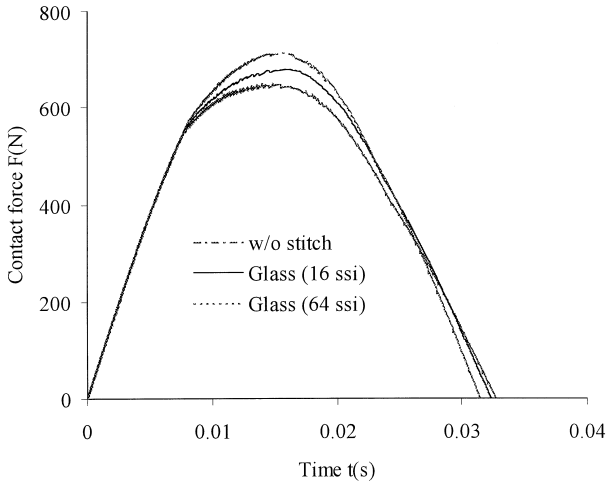

Fig. 8. Contact force F versus time t for $G_{\text{IIc}} = 530$ J/m^2.

Table 3
Contact force crack extension in various examples[a]

Example	h_1/H	Case	F_i (N)	$a_{\max}$ (mm)	$F_{\max}$ (N)
Example 1	0.5	w/o stitch	553	56.4	645
$T = 5.6125$ J		l6ssi	562	50.4	678
$G_{\text{IIC}} = 530$ J/m^2		64ssi	577	44.4	713
Example 2	0.5	w/o stitch	416	101.4	431
$T = 5.6125$ J		l6ssi	423	101.4	465
$G_{\text{IIc}} = 300$ J/m^2		64 ssi	438	59.4	679
Example 3	0.5	w/o stitch	553	56.4	645
$T = 5.6125$ J		l6ssi	562	50.4	678
$G_{\text{IIc}} = 530$ J/m^2		64ssi	577	44.4	712
Example 4	0.5	w/o stitch	545	27.4	545
$T = 2.813$ J		l6ssi	546	27.4	546
$G_{\text{IIc}} = 530$ J/m^2		64 ssi	548	27.4	546
Example 5	0.5	w/o stitch	416	49.4	478
$T = 2.813$ J		l6ssi	425	44.4	496
$G_{\text{IIc}} = 300$ J/m^2		64ssi	438	39.4	517
Example 6	0.25	w/o stitch	569	47.4	708
$T = 5.6125$ J		l6ssi	571	46.4	711
$G_{\text{IIc}} = 530$ J/m^2		64ssi	578	44.4	721
Example 7	0.25	w/o stitch	428	74.4	646
$T = 5.6125$ J		l6ssi	431	67.4	667
$G_{\text{IIc}} = 300$J/m^2		64 ssi	437	60.4	692
Example 8	0.25	w/o stitch	547	27.4	547
$T = 2.813$ J		l6ssi	548	27.4	548
$G_{\text{IIc}} = 530$ J/m^2		64 ssi	549	27.4	549
Example 9	0.25	w/o stitch	428	43.4	507
$T = 2.813$ J		l6ssi	431	41.4	511
$G_{\text{IIc}} = 300$ J/m^2		64ssi	437	40.4	518

[a] F, Contact force at crack initiation; $F_{\max}$, maximum contact force during the impact event; $a_{\max}$, crack length at the end of impact event.

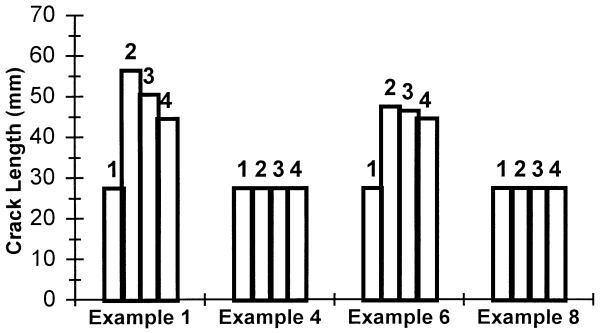

Fig. 9. Crack growth due to impact for $G_{IIc} = 530$ J/m^2. Bar 1, initial crack length; Bar 2, unstitched beam; Bar 3, 16 ssi stitches; Bar 4, 64 ssi stitches.

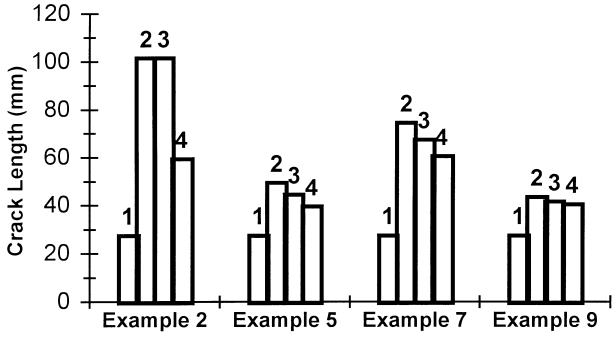

Fig. 10. Crack growth due to impact for $G_{IIc} = 300$ J/m^2. Bar 1, initial crack length, Bar 2, unstitched beam; Bar 3, 16 ssi stitches; Bar 4, 64 ssi stitches.

wherein $G_{IIc} = 530$ J/m^2 and Fig. 10 corresponds to $G_{IIc} = 300$ J/m^2.

There are many interesting observations that can be made from the results presented in Table 3. The contact force at which the delamination propagates is almost the same in unstitched and stitched beams. This initiation force depends only on the G_{IIc} and the position of the crack (h_1/H). Thus it does not depend on impact parameters such as impact energy. We have tacitly assumed that G_{IIc} is a constant independent of the loading rate.

In general, the extent of crack propagation at the end of the impact event is the least in the 64 ssi beam and the highest in the unstitched beams. The result for 16 ssi beams are somewhere in between. This can also be observed readily from the bar charts in Figs. 9 and 10. However the amount of delamination propagation depends also on the impact energy, G_{IIc} and h_1/H. Stitching is very effective in the beam with lower inherent fracture toughness. In Example 2 ($G_{IIc} = 300$ N/m) the crack propagates all the way to the ends of the beam in the unstitched and 16 ssi specimens, whereas the crack propagated up to $a = 59.4$ mm in the 64 ssi beam. In Example 1 ($G_{IIc} = 530$ N/m), the stitches were able to reduce the delamination extension by about 6–12 mm.

Stitches are also more effective when the crack is in the middle plane of the laminate ($h_1/H = 0.5$) compared to the cases wherein the crack is near the top surface of the beam ($h_1/H = 0.25$). This can be explained as follows. In an undelaminated beam, the shear stresses are higher at the midplane (1 .5 times the average shear stress) compared to the plane at 1/4 distance form the top. Thus, when the delamination is at the mid-plane the tendency for propagation is much higher. In fact the energy release rate G is higher for mid-plane delaminations. Thus the stitches play a very useful role in preventing crack propagation. This situation is similar to the effectiveness of stitches for various G_{IIc}s.

The stitches become more effective at higher impact energies when the propensity for crack propagation is also higher. This is because the stitches become active only if there is a delamination. Comparing Examples 1 and 4 in Fig. 9, one can see this phenomenon. In Example 4, the impact energy was very low so that stitching was not necessary. However, in Example 1, the effectiveness of stitch density could be inferred.

From the above discussion we can arrive at the following conclusions:

1. Static simulations of delaminated stitched beams provide an estimate of the apparent fracture toughness of the stitched laminates. The stitch density significantly affects the increase in apparent fracture toughness. The percentage increase is more for laminates with lower inherent fracture toughness.
2. The impact force at which the delamination begins to grow is not dependent on stitching. However, after the delamination growth is initiated, stitches come into play, and the extent of delamination growth depends on the stitching parameters. In general, the extent of crack propagation at the end of an impact event is small for higher stitch densities.
3. Stitching is effective when the impact energies are higher and the propensity for delamination growth is also higher.
4. Stitching is more effective when the delamination is at the center.

Acknowledgements

This research was supported by a grant from the National Science Foundation (Grant Number CMS-973 2887).

Appendix A. Derivation of force/displacement relations in the beam element

In this Appendix, the derivations for external forces F_{xi}, F_{zi} and moments C_i described in Section 2.3 are given.

Consider Part <1> of the beam shown in Fig. A1. P_i, V_i, and $M_i (i = 1, 2)$ are internal force and moment resultants and p_0 is shear force provided by stitches. The relations between external forces and internal force resultants the at left side of a beam and the right side of a beam are given as follows:

$$\begin{aligned} F_{x1} &= -P_1 \\ F_{z1} &= -V_1 \\ C_1 &= -M_1 \end{aligned} \tag{A1}$$

$$\begin{aligned} F_{x2} &= P_2 \\ F_{x2} &= V_2 \\ C_2 &= M_2 \end{aligned} \tag{A2}$$

Now we consider the internal force P in axial direction in the segment in Fig. A2.

The differential equations of equilibrium are:

$$A_1 E_1 \frac{\mathrm{d}^2 u}{\mathrm{d}x^2} = \frac{\mathrm{d}P}{\mathrm{d}x} = p_0 \tag{A3}$$

$$A_1 E_1 \frac{\mathrm{d}u}{\mathrm{d}x} = P \tag{A4}$$

Here, A_1 is area of cross-section of part <1>, E_1 is Young's modulus of part <1>. Substituting boundary condition at $x = 0$, $u = u_1$, at $x = a$, $u = u_2$ into Eqs. (A3) and (A4) and using the equations in (A1) and (A2), we have following expressions of F_{x1} and F_{x2}:

$$F_{x1} = \frac{A_1 E_1}{a}(u_1 - u_2) + \frac{p_0 a}{2} \tag{A5}$$

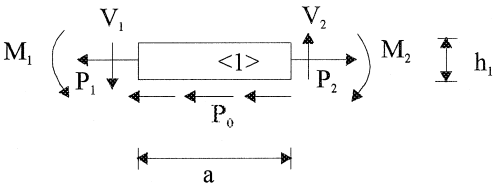

Fig. A1. Free body diagram in part <1>.

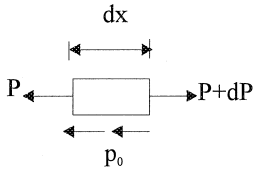

Fig. A2. Free body diagram in axial direction.

$$F_{x2} = \frac{A_1 E_1}{a}(u_2 - u_1) + \frac{p_0 a}{2} \tag{A6}$$

Consider the segment in Fig. A3 for deriving the expressions for F_{zi} and $C_i (i = 1, 2)$:

The M and V in an arbitrary cross-section can be expressed as:

$$E_1 I_1 \frac{\mathrm{d}\psi}{\mathrm{d}x} = M = M_1 + V_1 x - p_0 x \frac{h_1}{2} \tag{A7}$$

$$G_1 A_1 \left(\psi + \frac{\mathrm{d}w}{\mathrm{d}x}\right) = V = V_1 \tag{A8}$$

Here, I_1 is moment of inertia and G_1 is shear modulus of part <1>

At $x = 0$

$$w = w_1, \psi = \psi_1, V = V_1, M = M_1 \tag{A9}$$

At $x = a$

$$w = w_2, \psi = \psi_2, V = V_2, M = M_2 \tag{A10}$$

Solving Eqs. (A7) and (A8) and using boundary conditions in Eqs. (A9) and (A10), we can have the relations between V_i, M_i amd w_i, θ_i, then F_{zi} and C_i can be expressed in term of w_i, θ_i as given below:

$$F_{z1} = \frac{1}{A_1 a}\left(w_1 - \frac{a}{2}\psi_1 - w_2 - \frac{a}{2}\psi_2 - \frac{p_0 h_1 a^3}{23 E_1 I_1}\right) \tag{A11}$$

$$F_{z2} = \frac{1}{A_1 a}\left(-w_1 + \frac{a}{2}\psi_1 + w_2 + \frac{a}{2}\psi_2 + \frac{p_0 h_1 a^3}{23 E_1 I_1}\right) \tag{A12}$$

$$\begin{aligned} C_1 = &-\frac{w_1}{2A_1} + \psi_1\left(\frac{E_1 I_1}{a} + \frac{a}{4A_1}\right) + \frac{w_2}{2A_1} \\ &+ \psi_2\left(\frac{a}{4A_1} - \frac{E_1 I_1}{a}\right) + \frac{p_0 h_1 a^3}{48 E_1 I_1} - \frac{p_0 h_1 a}{4} \end{aligned} \tag{A13}$$

$$\begin{aligned} C_2 = &-\frac{w_1}{2A_1} + \psi_1\left(-\frac{E_1 I_1}{a} + \frac{a}{4A_1}\right) + \frac{w_2}{2A_1} \\ &+ \psi_2\left(\frac{a}{4A_1} + \frac{E_1 I_1}{a}\right) + \frac{p_0 h_1 a^3}{48 E_1 I_1} - \frac{p_0 h_1 a}{4} \end{aligned} \tag{A14}$$

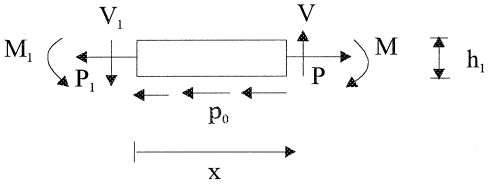

Fig. A3. Free body diagram in an arbitrary section.

where

$$A_1 = \frac{1}{G_1 A_1} + \frac{a^2}{12E_1 I_1}$$

Free body diagram of portion <2> is shown in Fig. A4.

The procedure for deriving the expressions for F_{xi}, F_{zi} and $C_i\,(i = 3, 4)$ is similar to that one in part <1>, and the results are:

$$F_{x3} = -\frac{p_0 a}{2} + \frac{A_2 E_2}{a}(u_3 - u_4) \tag{A15}$$

$$F_{x4} = -\frac{p_0 a}{2} + \frac{A_2 E_2}{a}(u_4 - u_3) \tag{A16}$$

$$F_{z3} = \frac{1}{A_2 a}\left(-\frac{p_0 h_2 a^3}{24E_2 I_2} + w_3 - \frac{\psi_3 a}{2} - w_4 - \frac{\psi_4 a}{2}\right) \tag{A17}$$

$$F_{z4} = \frac{1}{A_2 a}\left(\frac{p_0 h_2 a}{24E_2 I_2} - w_3 + \frac{\psi_3 a}{2} + w_4 + \frac{\psi_4 a}{2}\right) \tag{A18}$$

$$C_3 = -\frac{w_3}{2A_2} + \psi_3\left(\frac{a}{4A_2} + \frac{E_2 I_2}{a}\right) + \frac{w_4}{2A_2} + \psi_4\left(\frac{a}{4A_2} - \frac{E_2 I_2}{a}\right) + \frac{p_0 h_2 a^3}{48E_2 I_2 A_2} - \frac{p_0 h_2 a}{4} \tag{A19}$$

$$C_4 = -\frac{w_3}{2A_2} + \psi_3\left(\frac{a}{4A_2} - \frac{E_2 I_2}{a}\right) + \frac{w_4}{2A_2} + \psi_4\left(\frac{a}{4A_2} + \frac{E_2 I_2}{a}\right) + \frac{p_0 h_2 a^3}{48E_2 I_2 A_2} - \frac{p_0 h_2 a}{4} \tag{A20}$$

A_2 is area of cross-section, E_2 is Young's modulus and G_2 is shear modulus in part <2> and A_2 is given by:

$$A_2 = \frac{1}{G_2 A_2} + \frac{a^2}{12E_2 I_2}$$

The free body diagram of part <3> is shown in Fig. A5:

We can derive expressions for F_{xi}, F_{zi} and $C_i\,(i = 5, 6)$ as given below:

$$F_{x5} = \frac{A_3 E_3}{L}(u_5 - u_6) \tag{A21}$$

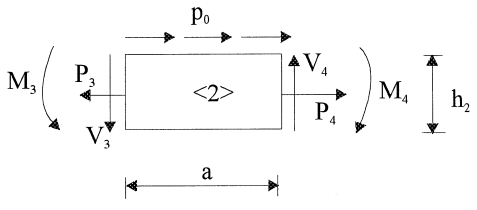

Fig. A4. Free body diagram in part <2>.

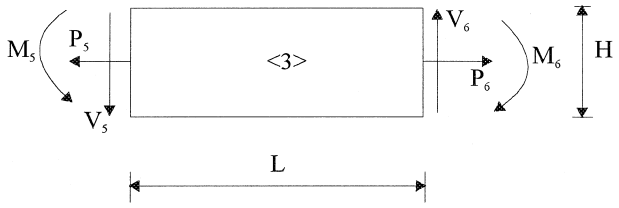

Fig. A5. Free body diagram in part <3>.

$$F_{x6} = \frac{A_3 E_3}{L}(u_6 - u_5) \tag{A22}$$

$$F_{z5} = \frac{w_5}{A_3 L} - \frac{\psi_5}{2A_3} - \frac{w_6}{A_3 L} - \frac{\psi_6}{2A_3} \tag{A23}$$

$$F_{z6} = -\frac{w_5}{A_3 L} + \frac{\psi_5}{2A_3} + \frac{w_6}{A_3 L} + \frac{\psi_6}{2A_3} \tag{A24}$$

$$C_5 = -\frac{w_5}{2A_3} + \left(\frac{E_3 I_3}{L} + \frac{L}{4A_3}\right)\psi_5 + \frac{w_6}{2A_3} + \left(-\frac{E_3 I_3}{L} + \frac{L}{4A_3}\right)\psi_6 \tag{A26}$$

$$C_6 = -\frac{w_5}{2A_3} + \left(-\frac{E_3 I_3}{L} + \frac{L}{4A_3}\right)\psi_5 + \frac{w_6}{2A_3} + \left(\frac{E_3 I_3}{L} + \frac{L}{4A_3}\right)\psi_6 \tag{A27}$$

A_3 is area of cross-section, E_3 is Young's modulus and G_3 is shear modulus in part <3>, and A_3 is given by:

$$A_3 = \frac{1}{G_3 A_3} + \frac{L}{12E_3 I_3}$$

Appendix B

The stiffness coefficients $k_{ij}(i = 1, 5, j = 1, 5)$ and the generalized forces $f_1 \ldots f_5$ on the right hand side of Eq. (18) are given as follows:

$$k_{12} = k_{15} = k_{21} = k_{23} = k_{25} = k_{32} = k_{51} = k_{52} = 0$$

$$k_{11} = \frac{1}{B_1 a} + \frac{1}{B_2 a}$$

$$k_{13} = k_{31} = -\frac{1}{B_1 a} - \frac{1}{B_2 a}$$

$$k_{14} = k_{41} = -\frac{1}{2B_1} - \frac{1}{2B_2}$$

$$k_{22} = \frac{A_1 E_1}{a} + \frac{A_2 E_2}{a}$$

$$k_{24} = k_{42} = \frac{A_1 E_1 h_2}{2a} - \frac{A_2 E_2 h_1}{2a}$$

$$k_{33} = \frac{1}{B_1 a} + \frac{1}{B_2 a} + \frac{1}{B_3 L}$$

$$k_{34} = k_{43} = \frac{1}{2B_1} + \frac{1}{2B_2} - \frac{1}{2B_3}$$

$$k_{35} = k_{53} = -\frac{1}{2B_3}$$

$$k_{44} = \frac{E_1 I_1}{a} + \frac{a}{4B_1} + \frac{E_2 I_2}{a} + \frac{a}{4B_2} + \frac{E_3 I_3}{L} + \frac{L}{4B_3} + \frac{A_1 E_1 h_2^2}{4a} + \frac{A_2 E_2 h_1^2}{4a}$$

$$k_{45} = k_{54} = \frac{L}{4B_3} - \frac{E_3 I_3}{L}$$

$$k_{55} = \frac{E_3 I_3}{L} + \frac{L}{4B_3}$$

$$f_1 = -\frac{F}{2} + \frac{p_0 h_1 a^2}{24 E_1 I_1 B_1} + \frac{p_0 h_2 a^2}{24 E_2 I_2 B_2}$$

$$f_3 = -\frac{p_0 h_2 a^2}{24 E_2 I_2 B_2} - \frac{p_0 h_1 a^2}{24 E_1 I_1 B_1}$$

$$f_4 = -\frac{p_0 h_1 a^3}{48 E_1 I_1 B_1} - \frac{p_0 h_2 a^3}{48 E_2 I_2 B_2}$$

$$f_2 = f_5 = 0$$

The expressions for B_1, B_2 and B_3 used in above expressions are as follows:

$$B_1 = \frac{1}{G_1 A_1} + \frac{a^2}{12 E_1 I_1}$$

$$B_2 = \frac{1}{G_2 A_2} + \frac{a}{12 E_2 I_2}$$

$$B_3 = \frac{1}{G_3 A_3} + \frac{L^2}{12 E_3 I_3}$$

Note that E_i and G_i are the equivalent Young's modulus and shear modulus, respectively, and A_i and I_i are area of cross-section and moment of inertia of the corresponding beam element.

References

[1] Chen L, Ifju PG, Sankar BV. A modified DCB test for composite laminates with high-density stitches. In: Proceedings of the American Society for Composites — Fourteenth Technical Conference. Lancaster (PA): Technomic Publishing Co., 1999. p. 456–65.

[2] Wallace BT, Sankar BV, Ifju PG. Delamination suppression in sandwich beams using trans-laminar reinforcements. In: Proceedings of the Aerospace Division. New York: American Society of Mechanical Engineers, 1999, p. 11–14.

[3] Sharma SK, Sankar BV. Effects of through-the-thickness stitching on impact and interlaminar fracture properties of textile graphite/epoxy laminates (NASA CR-195042). Washington (DC): National Aeronautics and Space Administration, 1995.

[4] Poe Jr. CC, Jackson WC, Portanova MA, Masters JE. Damage tolerance of textile composites. In: Proceedings of the Fourth NASA/DoD Conference, Salt Lake City, 7–11 June 1993.

[5] Dexter HB, Funk JG. Impact resistance and interlaminar fracture toughness of through-the-thickness reinforced graphite/epoxy (AIAA Paper 86-1 020-CP). Washington (DC): American Institute of Aeronautics and Astronautics, 1986.

[6] Pelstring RM, Madan RC. Stitching to improve damage tolerance of composites. In: 34th International SAMPE Symposium, Anaheim, CA, May 1989. p. 1519–82.

[7] Jain LK, Mai Y. On the effect of stitching on Mode I delamination toughness of laminated composites. Composites Science and Technology 1994;51:331–45.

[8] Sankar BV, Dharmapuri SM. Analysis of a stitched double cantilever beam. Journal of Composite Materials 1999;32(24):2203–25.

[9] Sonik V, Sankar BV. Modeling the effects of translaminar reinforcements on Mode H fracture toughness. In: Proceedings of the Aerospace Division, AD-vol. 52. New York: American Society of Mechanical Engineers, 1996. p. 61–9.

[10] Sankar BV, Sonik V. Modeling end-notched flexure tests of stitched laminates. In: Prodeedings of the American Society for Composites — Tenth Technical Conference. Lancaster (PA): Technomic Publishing Co., 1995, p. 172–81.

[11] Chen VL, Wu XX, Sun CT., Effective interlarninar fracture toughness in stitched laminates. In: Proceedings of the American Society for Composites — Eighth Annual Technical Conference. Lancaster (PA): Technomic Publishing Co., 1993, p. 453–62.

[12] Sankar BV. Low-velocity impact response and damage in composite laminates. In: Armanois E, editor. Fracture of composites. Zurich (Switzerland): Transtech Publications, Ltd, 1996. p. 555–82.

[13] Sankar BV. A finite element for modeling delaminations in composite beams. Computers & Structures 1991;38(2):239–46.

[14] Sankar BV, Sonik V. Pointwise energy release rate in delaminated plates. AIAA Journal 1995;33(7):1312–8.

[15] Sankar BV, Park O. Energy release rate calculations for laminated beams and plates. In: Proceedings of the American Society for Composites, 14th Technical Conference. Lancaster (PA): Technomic Publishing Co., 1999. p. 741–50.

[16] Sharma SK, Sankar BV. Mode H delamination toughness of stitched graphite/epoxy textile composites. Composite Science and Technology 1997;57(7):729–37.